



Simulation of dynamic orofacial movements using a constitutive law varying with muscle activation

Journal:	<i>Computer Methods in Biomechanics and Biomedical Engineering</i>
Manuscript ID:	GCMB-2009-0152.R1
Manuscript Type:	Special Issue Paper
Date Submitted by the Author:	
Complete List of Authors:	Nazari, Mohammad; Grenoble INP, GIPSA Lab Perrier, Pascal; Grenoble INP, CNRS UMR 5216, GIPSA-lab, Speech and Cognition Department Chabans, Matthieu; Grenoble INP, GIPSA-lab, Speech and Cognition Department Payan, Yohan; Université Joseph Fourier - CNRS UMR 5525, Equipe GMCAO - Laboratoire TIMC-IMAG
Keywords:	face biomechanics, orofacial movements, muscle active force, hyperelastic modelling



Simulation of dynamic orofacial movements using a constitutive law varying with muscle activation

NAZARI Mohammad Ali^{1,2}, PERRIER Pascal¹, CHABANAS Matthieu¹ and PAYAN Yohan³

1. GIPSA-lab, Speech and Cognition Department, CNRS UMR 5216 / Grenoble Institute of Technology, France

2. Mechanical Engineering Department, Faculty of Engineering, University of Tehran, Iran

3. TIMC-IMAG, CNRS UMR 5525 / Université Joseph Fourier, Grenoble, France¹

Correspondance: Mohammad Ali NAZARI, GIPSA-lab Département Parole & Cognition, Domaine universitaire BP 46, 38402 Saint Martin d'Hères, France

This paper presents a biomechanical model of the face to simulate orofacial movements in speech and non-verbal communication. A 3D finite element model, based on medical images of a subject, is presented. A hyperelastic Mooney-Rivlin constitutive law accounts for the non linear behaviour of facial tissue. Muscles fibres are represented by piece-wise uniaxial tensile elements, which generate force. The stress stiffening effect, an increase of the stiffness of the muscles when activated, is modelled by varying the constitutive law of the tissue with the level of activation of the muscle. A large number of facial movements occurring during speech and facial mimics are simulated. Results show that our modelling approach provides a realistic account of facial mimics. The differences between dynamic versus quasi-static simulations are also discussed, proving that dynamic trajectories better fit experimental data.

Keywords: face biomechanics; orofacial movements; muscle active force; hyperelastic modelling.

1. Introduction

Orofacial gestures, produced by articulators such as the tongue, jaw and lips, are of primary importance in speech communication. By their position at the extremity of the vocal tract, lips have a major influence on the acoustic signal generated by the airflow coming from the lung. In addition, seeing facial gestures directly influence the perception of speech. Listeners perceive and interpret the produced speech via a combination of auditory and visual processing, a strategy well demonstrated by the well-know McGurk effect (McGurk and MacDonald 1976).

¹ Currently in PIMS, CNRS UMI 3069 / University of British Columbia, Vancouver, Canada

1
2
3
4
5
6
7
8
9
10
11
12
13
14
15
16
17
18
19
20
21
22
23
24
25
26
27
28
29
30
31
32
33
34
35
36
37
38
39
40
41
42
43
44
45
46
47
48
49
50
51
52
53
54
55
56
57
58
59
60

Consequently an important field in speech communication research is the development of synthetic models of the human face. The accuracy of these models is a major requirement, both for production and perception of speech. In this context, due to the strong influence of 3D lip horn geometry on the spectral characteristics of speech signals, special attention has to be devoted the modelling of the lips region. Moreover, it has been shown that the dynamic of the movements is very important in the perception of facial expressions (Munhall and Vatikiotis-Bateson 1998; Ambadar et al. 2005). Hence, synthetic speaking faces have to well account for the temporal course of face shaping.

Contrary to empirical models based on recorded data or medical images (for example Lucero et al. (2005) or Badin et al. (2008)), our approach in the last decade has been to develop biomechanical models of speech articulators, which are as close as possible to the human anatomy and functional morphology. Special emphasis has been given to the representation of the muscular structures and the rheological properties of soft tissues. Another major contribution has dealt with the motor control system involved in the production of speech and orofacial movements: which muscles have to be contracted to obtain a given acoustic signal or facial mimic? What must be the intensities, variations and sequencing of the motor commands? Former works were focused on a biomechanical modelling of the tongue, first in 2D then in 3D, and the controlled activation of its muscles to generate complex articulatory paths (Payan and Perrier 1997; Perrier et al. 2003; Buchaillard et al. 2009). In continuation of these works, this paper presents a biomechanical model of the face which enables the generation of facial movements in response to muscles activations. The bases of the finite element model (mesh, mechanical properties and boundary conditions), which represent the passive tissues of the face, are presented in section 2. Then, section 3 is

1
2
3 entirely focused on the active components, namely the muscles: their representation,
4 mechanism of contraction, and the evolution of their mechanical properties with
5 activation. Simulations of different orofacial movements are presented in section 4,
6 before the discussion and conclusion.
7
8
9

10 11 12 13 14 **2. Main structure of the model**

15
16 Many physically-based models of the human face were developed in the
17 framework of computer graphics facial animation (Lee et al. 1995; Sifakis et al.
18 2005), computer aided surgery (Chabanas et al. 2003; Gladilin et al. 2004) or speech
19 production study (Lucero and Munhall 1999; Gomi et al. 2006).
20
21
22
23
24

25
26 The pioneer work of Lee et al. (1995) has made popular a discrete modelling
27 framework, with sparse mass-spring entities regularly assembled inside facial tissues.
28 This approach allows fast computations with a simple algorithmic implementation.
29 However, in addition to the lack of accuracy of such models and to their numerical
30 instabilities, it seems to be very difficult to set their elastic parameters (the stiffness of
31 springs) in order to fit the constitutive behaviour that is observed and measured on
32 living tissues. Recently Kim & Gomi (2007) have improved Gomi et al.'s (2006)
33 discrete model by implementing a so-called "continuum compatible" mass-spring
34 model with stiffness parameters that can be adjusted in order to follow a simple linear
35 continuum constitutive law. Although this model is interesting in computational
36 terms, especially for dynamic simulations, it is limited to correctly reproduce the
37 behaviour of highly non-linear material such as facial tissues (Fung 1993; Gerard et
38 al. 2005).
39
40
41
42
43
44
45
46
47
48
49
50
51
52
53
54
55

56
57 In continuity with the works of Chabanas et al. (2003) and Sifakis et al.
58 (2005), we have chosen to use the Finite Element method to model the continuous
59 tissues of the human face (Groleau et al. 2007; Nazari et al. 2008). Although
60

1
2
3 computationally less efficient, it enables in particular the use of non linear mechanical
4 modelling such as hyperelastic laws to better approximate the tissues behaviour
5
6 (Humphrey and Yin 1989; Weiss et al. 1996; Yucesoy et al. 2002; Blemker et al.
7
8 2005).
9

10
11
12 Our implementation is based on the ANSYS ® release 11.0 software.
13

14 15 16 **2.1 Mesh of the passive tissues** 17

18
19 The main mesh is a Finite Element (FE) discretization of the volume defined
20 by the facial tissues located between the skull and the external skin surface of the
21 face. It is based on a previous continuous face model developed by Chabanas et al.
22 (2003) in the context of computer aided maxillo-facial surgery. The outer and inner
23 surfaces of the mesh were extracted from a CT scan of a female adult subject. The
24 volume delimited by these two surfaces was then manually meshed, as regularly as
25 possible, with hexahedral and wedge elements (figure 1). Anatomically, the face can
26 be considered as the superposition of three distinct layers of tissues, namely (from the
27 internal to the external layer) the hypodermis, dermis and epidermis (Stranding 2005).
28 The mesh is thus also built in three discrete layers of elements. The external one
29 corresponds to the epidermis (very thin) and dermis parts while the two internal layers
30 model the hypodermis, which will later include the facial musculature (section 3). The
31 mesh is composed of 6342 brick elements (6024 hexahedron and 318 wedges) based
32 on 8720 nodes. In order to reduce the number of DOF during simulation the mesh was
33 assumed to be symmetrical along the sagittal plane, which seems reasonable in the
34 context of speech production.
35
36
37
38
39
40
41
42
43
44
45
46
47
48
49
50
51
52
53
54
55

56
57
58 ----- Figure 1 around here -----
59
60

2.2 Mechanical properties

Element material properties are assumed to follow a hyperelastic law (Fung 1993). A simplified 5 parameters Mooney-Rivlin model is used, which is based on a strain-energy function W defined by:

$$W=c_{10}(I_1-3)+c_{01}(I_2-3)+c_{20}(I_1-3)^2+c_{11}(I_1-3)(I_2-3)+c_{02}(I_2-3)^2+((J-1)^2/d) \quad (1)$$

where I_1 and I_2 are respectively the first and second invariants of the right Cauchy-Green strain tensor, J is the determinant of the elastic deformation gradient, and $d=(1-2\nu)/(c_{10}+c_{01})$ with ν the Poisson's ratio. The derivatives of W with respect to strain give stress:

$$S_{ij}=2\partial W/\partial C_{ij} \quad (2)$$

S_{ij} are the components of the second Piola-Kirchhoff stress tensor and C_{ij} the components of the right Cauchy-Green deformation tensor.

In our work, a simplified version of the strain-energy function W is used with only two constants, c_{10} and c_{20} , different from zero (Gerard et al. 2005; Buchaillard et al. 2009). According to Tracqui and Ohayon (2004), $c_{10}\approx E/6$ where E is the Young's modulus. The two coefficients c_{10} and d have been calculated from the values reported in Payan and Perrier (1997), with the assumption of mechanical linearity and incompressibility of tissues, namely $E=15$ kPa and $\nu=0.499$. The c_{20} coefficient has been adapted from the values proposed for tongue tissues by Buchaillard et al. (2009) based on indentation measures from a cadaver's tongue (Gerard et al., 2005). The computed constants are shown in table 1.

----- Table 1 around here -----

The modelled passive tissues have been so far considered as homogeneous and isotropic. It could be improved in future works, especially by setting specific

1
2
3 mechanical properties to the different layers of the mesh. The mechanical properties
4 of the active part of the model, the muscles, will be treated in section 3.4.
5
6
7
8
9

10 **2.3 Boundary conditions and contact surfaces**

11
12 Nodes of the internal layer of the mesh corresponding to the face tissue
13 attachments to the skull are fixed. Others are free.
14

15
16 During speech and facial mimics, many contacts occur between the upper and
17 lower lip, and between the lips and the teeth. They are extremely important in lips
18 shaping. The teeth surfaces on mandible and maxilla, segmented on CT images, have
19 been approximated with spline surfaces, and then meshed with quadrilateral
20 undeformable elements (figure 2). Contacts are handled using surface to surface
21 contact elements (CONTA173 and TARGE170 in Ansys ®), which provide collision
22 detection and sliding reaction, considered here without friction ($\mu=0$). There is no
23 initial interpenetration between all the contact surfaces.
24
25
26
27
28
29
30
31
32
33
34
35
36
37

38 ----- Figure 2 around here -----
39
40

41 **3. Muscles**

42
43 Since orofacial movements are directly generated by facial muscles, a realistic
44 modelling of their course and mechanical properties is a main challenge. The total
45 force generated in a muscle is the sum of two components: an active (F_{ac}) one and a
46 passive (F_{pc}) one. Due to α -motoneurons depolarization, muscle fibres generate force,
47 which in turn causes change in muscle length. The force generated through the actin-
48 myosin cross-bridges is the active component of muscle force. Due to their stiffness
49 the surrounding tissues will resist to the active component thus defining a passive
50 component of muscle force. In real muscles this passive component is not isotropic
51
52
53
54
55
56
57
58
59
60

1
2
3 since the mechanical properties in the direction of muscle collagen fibres are different
4
5 from the embedding matrix (McMahon 1984). Hence, the passive material behaviour
6
7 should be modelled with a transversely isotropic material (Humphrey and Yin 1989;
8
9 Weiss et al. 1996; Yucesoy et al. 2002; Blemker et al. 2005). However, in a first
10
11 approach, this behaviour is considered as isotropic.
12
13

14
15 The very earlier model of the active part of muscle force was proposed by
16
17 Hill (1938). According to this basic model a contractile element generates force as a
18
19 function of muscle length (F versus L curve) and its velocity (F versus V curve).
20
21 These curves are assumed to be scaled up or down as a function of the level of
22
23 activation (Zajac 1989). More recently, authors working with finite element
24
25 framework have modelled the muscle force by designing new elements which include
26
27 both active stress stiffening effect and passive transversal isotropy (Wilhelms-Tricario
28
29 1995; Blemker et al. 2005). These elements need to be oriented along the axis of
30
31 isotropy (Ng-Thow-Hing and Fiume 2002) to define fibre and cross fibre directions
32
33 and also they should be distinguished from the surrounding tissues (Teran et al. 2005).
34
35 This method has been implemented by Sifakis et al. (2006) for modelling face
36
37 muscles and speech behaviours quasi-statically.
38
39
40
41
42

43
44 Next subsections present the muscle modelling developed in our work, with
45
46 the representation of their active and passive components and the stress stiffening
47
48 effect, leading to an evolution of the mechanical properties of muscles during
49
50 contraction.
51
52

53 ***3.1 Muscle contractile fibres or active part***

54
55
56 The muscular structure of the face enables huge possibilities of movements, in
57
58 speech, eating and facial expressions, with a great dexterity. Its complex structure can
59
60 be divided in two groups of muscles (Stranding 2005). Muscles of mastication are the

1
2
3 deep, strong muscles that generate the movement of the mandible. Since the mandible
4 is not handled yet in our modelling, we have only focused on the other group, the
5 muscles of the lip region, namely the superficial muscles involved in facial mimics
6 (Hardcastle 1976). Most of them are bilateral, symmetrical, gathered around the lips
7 with one bony insertion and the other within the facial tissues. A notable exception is
8 the orbicularis oris, a specific constrictor muscle embedded in the lips without bony
9 insertions.
10
11
12
13
14
15
16
17
18

19
20 In order to ensure anatomical and physical reliability, muscles courses and
21 insertions were directly defined from medical images and anatomical charts, with the
22 help of a maxillofacial surgeon. The locations of points describing the muscle fibres
23 were measured in the different CT scan slices. The number of fibres per muscle
24 depends on its extent and size. Figure 3 and table 2 show the ten orofacial muscles
25 that are modelled.
26
27
28
29
30
31
32
33

34
35 ----- Figure 3 around here -----
36

37 ----- Table 2 around here -----
38
39

40 Muscle fibres are embedded in the facial mesh as continuous sets of uniaxial
41 cable elements. Since each cable is a line in 3D space, their number per fibre
42 increases as a function of the muscle fibre curvature, to model this curvature
43 smoothly. These cable elements (LINK10 in Ansys®) act in tension only and will
44 become slack under compression. Such properties are consistent with the observations
45 that in the fibre direction a muscle can resist only tensile forces and not compressive
46 forces (Loocke et al. 2006).
47
48
49
50
51
52
53
54
55

56 End points of the cable elements are defined independently of the level of
57 refinement of the main mesh. They correspond to anatomical landmarks located in
58 reference to the skull. This approach enables to refine or modify the mesh without
59
60

1
2
3 requiring any change in the definition of muscles courses. To couple the fibres with
4 the main mesh, *point to surface* contact elements are used. The *points* (pilot nodes)
5 are the extremities of the cable elements. They are bilaterally linked to the *surfaces* of
6 the mesh elements which centroids are the closest to the cable extremity. Figure 4
7 displays the cable elements and the corresponding coupling elements for the muscles
8 in half of the face. The no-displacement boundary condition is also applied to the ends
9 of cable elements that correspond to the muscles insertions on the skull.
10
11
12
13
14
15
16
17
18
19

20 ----- Figure 4 around here -----
21
22

23 **3.2 Muscle body or passive part**

24
25
26
27 Once the fibres are set, the body of the muscles can be defined in the main
28 mesh. A neighbourhood is determined around each fibre by an algorithm considering
29 a sphere, which radius is equal to an estimation of the muscle cross-sectional
30 dimension, running along the cable elements lines. Each element of the main mesh
31 intersecting the sphere is then labelled as a part of the muscle body. The resulting
32 bodies of the muscles in the mesh are displayed in figure 5 for the left half of the face.
33
34
35
36
37
38
39
40
41 Although this definition of the muscle body is a rough approximation, it is enough so
42 far for our use, which is to account for the stress stiffening effect.
43
44
45
46
47
48
49

50 ----- Figure 5 around here -----
51
52

53 **3.3 Stress stiffening effect**

54
55
56
57
58
59
60
Muscles behave like a transversely isotropic material, with an isotropic
behaviour in the directions orthogonal to the muscle fibres. This means that
mechanical properties in the direction of muscle fibres are different from the ones in
the cross-fibre direction. Due to force generation in the fibres direction and to the

fibres tensile characteristics, the transversal bending stiffness increases with the tensile force (similarly to the stress stiffening phenomenon in cable members or membranes).

----- Figure 6 around here -----

This is illustrated in Figure 6 with a simple example of a virtual point P inside a muscle fibre originally at equilibrium under constant muscle activation (force F_l) and then displaced (by δ) because of the action of a force F applied in the muscle transversal direction. Once the new equilibrium is reached (Figure 6 lower panel), assuming a linear relationship between force and displacement, we have:

$$F = 2F_l \frac{\delta}{\ell_1} \left(\frac{1}{\sqrt{1 + \left(\frac{\delta}{\ell_1}\right)^2}} \right) \quad (3)$$

This means that, when δ is negligible as compared to ℓ_1 , the muscle transversal stiffness $dF/d\delta$ is proportional to muscle force F_l .

When a muscle is activated, its fibres generate forces that resist to elongation, according to a certain tension-length relation (see for example McMahon (1984)), and in a way that increases when activation increases (see for example Wilhelms-Tricario (1995)). In real muscle the fibres distribution is so dense, that the resistance to elongation of the whole muscle body increases with elongation in the fibres direction. In our model, muscle fibres are not represented in all their details. They are modelled by a limited number of *localized* macrofibres (typically from one to three). When the muscle is activated, each of these macrofibres generates a force and resists to the elongation, but since the fibres are localized, this resistance does not apply to the whole body of the muscle. This would not be a realistic behaviour. In order to compensate for this drawback, the stiffness in the body elements of the muscles

(section 3.2) increases with muscle activation in the fibres directions. Hence, muscle activation is associated both with a resistance to stress in the direction orthogonal to the fibre direction (the stress stiffening effect) and with a resistance to elongation in the fibre direction. Consequently, it is modelled by an isotropic increase of the tissues stiffness, implemented by modifying the parameters of the passive constitutive law (equation 1), according to the approach explained in the next section.

3.4 Implementation of muscle activation and stress stiffening effect

The cable elements generate the active force F_{ac} of each muscle, following the relation:

$$F_{ac} = AE_{cable} (\varepsilon - \alpha \Delta T) \quad (4)$$

where A is the cable cross sectional area, ε its strain and E_{cable} its Young's modulus. In standard ANSYS ® use, parameter T is equivalent to the temperature of the element, and α to the thermal coefficient of expansion of the cable. In our case, we have used parameters T and E_{cable} to specify the *level of activation*. Parameter E_{cable} is a scaling factor specifying the maximal level of activation, which is muscle specific. Parameter T is used to control the *level of activation* within the muscle specific maximal range of variation. Thus, parameter T can be considered as a *normalized control parameter of muscle activation*. Decreasing T leads to a shortening of the cables lengths, which therefore exert forces on the main mesh through the coupling elements. The activation level is then a decreasing function of parameter T . The value of α is arbitrarily set to 0.001

To account for the stress stiffening effect, the constitutive law of the elements of a muscle body varies with the level of muscle activation specified with T . In agreement with Buchaillard et al. (2009), parameters c_{10} and c_{20} of the passive

1
2
3 hyperelastic law are hence linearly scaled as an increasing function of the activation,
4
5 which is a decreasing function of T (Figure 7).
6
7

8
9 ----- Figure 7 around here -----
10

11
12 When different muscles are activated simultaneously, the stiffness of the main
13 mesh elements which are common to these muscles' bodies change as a function of
14 the most activated muscle, and not as the result of an accumulation of the stiffness
15 changes associated with each individual muscle activation. The proposed stress
16 stiffening modelling is functionally correct, except for the resistance to compression
17 in the fibres direction. Indeed, it is known that this resistance varies with the strain
18 rate and is close to zero when this rate is low (Loocke et al. 2006). Further
19 improvements will be provided along this line in future works.
20
21
22
23
24
25
26
27
28
29
30

31
32 The muscle activation varies in time as a ramp function. In further works that
33 we will develop in the context of speech production, these commands will be handled
34 by a motor control mechanism integrating voluntary commands and low-level
35 feedback information sent by the muscles (Feldman 1986; Buchaillard et al. 2006).
36
37
38
39
40
41

42 **3.5 Dynamic parameters**

43
44 For dynamic transient analysis, viscosity is modelled using proportional
45 damping:
46
47

$$48 \mathbf{C} = \alpha \mathbf{M} + \beta \mathbf{K} \quad (5)$$

49
50 To determine α and β coefficients the first 7000 modes of the main mesh (about a
51 third of the total number of degrees of freedom) were calculated. Simulations were
52 run twice, first with the material stiffness used in the absence of muscle activation and
53 then for a high material stiffness level (10 times more). The corresponding natural
54 frequencies vary from 0.5 Hz up to 15 Hz. Within this interval, parameters α and β
55
56
57
58
59
60

1
2
3 have been tuned such that the damping ratio (ratio of viscous damping factor to
4 critical damping) is larger than and near to one. The computed values are $\alpha=19 \text{ sec}^{-1}$
5
6 and $\beta=0.055 \text{ sec}$.
7
8
9

10 The density of face tissues is set to $\rho=1.04E^{-6} \text{ kg/mm}^3$ (Buchaillard et al.
11 2006). The effect of gravity has not been considered.
12
13

14 Other parameters regarding solver and computational costs are discussed in
15 the appendix.
16
17
18
19

20 21 22 **4. Simulations and results** 23

24 Different muscle activation patterns have been used and their influences on facial
25 gestures and mimics evaluated. Both static and transient analyses have been
26 performed. In addition to the static analysis that takes into account only the stiffness
27 matrix, dynamic simulations obtained with full transient analysis also takes into
28 account the effect of inertia and viscosity.
29
30
31
32
33
34
35

36 37 38 **4.1 Simulation of facial mimics resulting from various orofacial gestures** 39

40 Activation of muscles taken individually and in coordination has been
41 investigated. In this section, only the final shapes of the mesh resulting from these
42 activations are shown. They are the same for the static and the full transient analysis.
43 These results well comply with the anatomical predictions in the related literature
44 (Standing 2005).
45
46
47
48
49
50

51 The result of activating zygomaticus draws the angle of the mouth upwards
52 and laterally (Figure 8).
53
54
55

56
57
58 ----- Figure 8 around here -----
59
60

1
2
3 Levator labii superioris elevates the upper lip. Acting with other muscles, it modifies
4 the nasolabial furrow. In some faces, this furrow is a highly characteristic feature
5 often deepened in expressions of sadness or seriousness. The activation of the levator
6 labii superioris with zygomaticus and levator labii superioris alaeque nasi in Figure 9
7 well satisfies that hypothesis.
8
9

10
11
12
13
14
15
16 ----- Figure 9 around here -----
17

18
19
20 The effect of orbicularis oris peripheralis (OOP) in protruding and rounding
21 the lips has been shown (Figure 10). The effect of stiffening in producing rounding
22 with protrusion has been discussed in Nazari et al. (2008): without the stiffening, lips
23 are protruded but the amount of lip opening is too large.
24
25
26
27
28
29

30
31 ----- Figure 10 around here -----
32
33

34 Figure 11 shows the consequence of the activation of the risorius and Figure
35 12 the impact of activation of the buccinator (BUC). In Figure 13 the mimic
36 associated with the coordinated action of OOP and BUC is illustrated. In all these
37 figures these actions are qualitatively consistent with predictions made from
38 anatomical knowledge.
39
40
41
42
43
44

45
46
47 ----- Figure 11 around here -----
48
49

50
51 The risorius is known to stretch the mouth laterally and to retract the corners of the
52 mouth. This is consistent with the strain depicted in Figure 11. The buccinator has no
53 or little influence on the lips, and essentially compresses the cheeks against the teeth
54 (Blanton et al. 1970). Our simulation matches quite well these expectations (Figure
55
56
57
58
59
60

1
2
3 12): the lips have the same shape as in our model at rest, while the strain essentially
4
5 affects the lower part of the face.
6
7

8
9 ----- Figure 12 around here -----
10

11
12 The OOP has been shown in our model to generate a protrusion and a closing of the
13 lips which is consistent with usual hypotheses in the literature (Gomi et. al 2006;
14 Nazari et. al 2008). Meanwhile, the coordinated action of the buccinator and the OOP
15 generates a closing of the lips only. It can be assumed that the stiffening of the cheeks
16 due to the buccinator activation limits the amplitude of the lip protrusion, which
17 would explain that mainly closure is observed.
18
19
20
21
22
23
24
25
26

27
28 ----- Figure 13 around here -----
29

30 ***4.2 Dynamics versus Quasi-static simulations*** 31

32
33
34 We have studied the effect of dynamic versus quasi-static analysis on the lip
35 protrusion. For this purpose both OOP and mentalis (MENT) muscles are activated.
36 The same activation level in both dynamic and static analyses is assumed. Figure 14
37 shows the trajectories, for both conditions, of a node located on the lower lip in the
38 midsagittal plane.
39
40
41
42
43
44
45

46
47 ----- Figure 14 around here -----
48

49 While starting and ending points are the same in static and dynamic analysis, the
50 trajectories are clearly different. The trajectory obtained with the static analysis is
51 close to a straight line while the dynamic trajectory is noticeably curved. This
52 difference is large enough to generate significant differences in lip shape variation
53 from the starting point to the ending point, and then to significantly influence the
54
55
56
57
58
59
60

1
2
3 acoustic signal. In addition, a large number of human skilled movements have been
4
5 shown to follow curved path (Morasso, 1981).
6
7

8 Figure 15 shows the tangential velocity profile for the same point together
9
10 with the corresponding activation signal..
11
12

13
14 ----- Figure 15 around here -----
15
16

17 An asymmetrical bell-shaped velocity pattern is generated. This kinematic
18 pattern is typical for lip movements as shown for example by Shaiman et al. (1997)
19 for several American English speakers.
20
21
22
23

24 Both properties, the curved path and the bell-shaped velocity profiles,
25 observed in experimental studies and accounted for in dynamic analysis and not in
26 quasi-static analysis demonstrates the necessity to integrate dynamic factors, such as
27 inertia and damping, to obtain realistic simulations of lip shape variations in speech
28 production.
29
30
31
32
33
34

35 To assess more precisely the realism of the trajectories produced by our
36 model, they can be compared to lips trajectories measured with video processing
37 (Abry et al. 1996) from a native speaker of French. As an illustration, let us consider
38 the sequence /iRy/ embedded in the carrier sentence 'Tu dis "ruise" (/tydiRyiz/, you're
39 saying "ruise", /). These data were processed with a low-pass linear phase filter (cut-
40 off frequency 6 Hz). The trajectory of a point located on the lower lip in the mid-
41 sagittal plane has been extracted in the temporal section corresponding to lip
42 protrusion from /i/ to /y/ (Figure 16). It can be observed that the path of this point is
43 qualitatively similar to the path simulated with dynamic analysis (Figure 14). More
44 specifically, the path is curved, a key feature that could not be predicted from the
45 pseudo-static analysis.
46
47
48
49
50
51
52
53
54
55
56
57
58
59
60

1
2
3
4
5 ----- Figure 16 around here -----
6
7
8

9
10 Figure 17 shows the experimental velocity profile: it has, like our simulation,
11 an asymmetrical bell-shape in agreement with Shaiman et al.'s (1997) data collected
12 from speakers of American English.
13
14

15
16
17
18 ----- Figure 17 around here -----
19
20

21
22
23 This example of a comparison between simulations and real data confirms the general
24 observation made above: contrary to those obtained in the quasi-static analysis
25 framework, the simulations obtained in the dynamic analysis framework generate
26 curved paths and bell-shaped velocity profiles similar to those observed in
27 experimental lips protrusion movements collected during speech production
28
29
30
31
32
33

34
35 The experimental movement and the simulation in dynamic analysis have also
36 similar ranges of velocity (maximum velocity 3.9cm/s *versus* 2.4cm/s), durations
37 (200ms *versus* 270ms at 20% of the peak velocity), and movement amplitudes
38 (4.5mm *versus* 4mm for the horizontal protrusion).
39
40
41
42
43

44
45 Some discrepancies can be noticed between simulations and experimental
46 data. In the experimental data, the curved path includes a rising part followed by a
47 short decline. In the simulation this rising/declining sequence is also observed, but it
48 is preceded by a horizontal part. It is important to state that these differences are not
49 intrinsically due to the characteristics of the model but, more factually, to differences
50 between the conditions of simulation and the conditions of real speech production. In
51 the simulations the movement starts from a zero velocity position and ends at a zero
52 velocity position, while experimental data were extracted from a longer speech
53
54
55
56
57
58
59
60

1
2
3 continuum (Figure 16) in which the observed section does not start or end with a zero
4
5
6 velocity position. This phenomenon can be clearly seen in the experimental velocity
7
8 profile (Figure 17), in which velocity curve never crosses zero.
9

10 11 12 13 14 **5. Discussion and conclusion**

15
16
17 The use of a realistic dynamical biomechanical model of the face has allowed
18
19
20
21
22
23
24
25
26
27
28
29
30
31
32
33
34
35
36
37
38
39
40
41
42
43
44
45
46
47
48
49
50
51
52
53
54
55
56
57
58
59
60
61
62
63
64
65
66
67
68
69
70
71
72
73
74
75
76
77
78
79
80
81
82
83
84
85
86
87
88
89
90
91
92
93
94
95
96
97
98
99
100
101
102
103
104
105
106
107
108
109
110
111
112
113
114
115
116
117
118
119
120
121
122
123
124
125
126
127
128
129
130
131
132
133
134
135
136
137
138
139
140
141
142
143
144
145
146
147
148
149
150
151
152
153
154
155
156
157
158
159
160
161
162
163
164
165
166
167
168
169
170
171
172
173
174
175
176
177
178
179
180
181
182
183
184
185
186
187
188
189
190
191
192
193
194
195
196
197
198
199
200
201
202
203
204
205
206
207
208
209
210
211
212
213
214
215
216
217
218
219
220
221
222
223
224
225
226
227
228
229
230
231
232
233
234
235
236
237
238
239
240
241
242
243
244
245
246
247
248
249
250
251
252
253
254
255
256
257
258
259
260
261
262
263
264
265
266
267
268
269
270
271
272
273
274
275
276
277
278
279
280
281
282
283
284
285
286
287
288
289
290
291
292
293
294
295
296
297
298
299
300
301
302
303
304
305
306
307
308
309
310
311
312
313
314
315
316
317
318
319
320
321
322
323
324
325
326
327
328
329
330
331
332
333
334
335
336
337
338
339
340
341
342
343
344
345
346
347
348
349
350
351
352
353
354
355
356
357
358
359
360
361
362
363
364
365
366
367
368
369
370
371
372
373
374
375
376
377
378
379
380
381
382
383
384
385
386
387
388
389
390
391
392
393
394
395
396
397
398
399
400
401
402
403
404
405
406
407
408
409
410
411
412
413
414
415
416
417
418
419
420
421
422
423
424
425
426
427
428
429
430
431
432
433
434
435
436
437
438
439
440
441
442
443
444
445
446
447
448
449
450
451
452
453
454
455
456
457
458
459
460
461
462
463
464
465
466
467
468
469
470
471
472
473
474
475
476
477
478
479
480
481
482
483
484
485
486
487
488
489
490
491
492
493
494
495
496
497
498
499
500
501
502
503
504
505
506
507
508
509
510
511
512
513
514
515
516
517
518
519
520
521
522
523
524
525
526
527
528
529
530
531
532
533
534
535
536
537
538
539
540
541
542
543
544
545
546
547
548
549
550
551
552
553
554
555
556
557
558
559
560
561
562
563
564
565
566
567
568
569
570
571
572
573
574
575
576
577
578
579
580
581
582
583
584
585
586
587
588
589
590
591
592
593
594
595
596
597
598
599
600
601
602
603
604
605
606
607
608
609
610
611
612
613
614
615
616
617
618
619
620
621
622
623
624
625
626
627
628
629
630
631
632
633
634
635
636
637
638
639
640
641
642
643
644
645
646
647
648
649
650
651
652
653
654
655
656
657
658
659
660
661
662
663
664
665
666
667
668
669
670
671
672
673
674
675
676
677
678
679
680
681
682
683
684
685
686
687
688
689
690
691
692
693
694
695
696
697
698
699
700
701
702
703
704
705
706
707
708
709
710
711
712
713
714
715
716
717
718
719
720
721
722
723
724
725
726
727
728
729
730
731
732
733
734
735
736
737
738
739
740
741
742
743
744
745
746
747
748
749
750
751
752
753
754
755
756
757
758
759
760
761
762
763
764
765
766
767
768
769
770
771
772
773
774
775
776
777
778
779
780
781
782
783
784
785
786
787
788
789
790
791
792
793
794
795
796
797
798
799
800
801
802
803
804
805
806
807
808
809
810
811
812
813
814
815
816
817
818
819
820
821
822
823
824
825
826
827
828
829
830
831
832
833
834
835
836
837
838
839
840
841
842
843
844
845
846
847
848
849
850
851
852
853
854
855
856
857
858
859
860
861
862
863
864
865
866
867
868
869
870
871
872
873
874
875
876
877
878
879
880
881
882
883
884
885
886
887
888
889
890
891
892
893
894
895
896
897
898
899
900
901
902
903
904
905
906
907
908
909
910
911
912
913
914
915
916
917
918
919
920
921
922
923
924
925
926
927
928
929
930
931
932
933
934
935
936
937
938
939
940
941
942
943
944
945
946
947
948
949
950
951
952
953
954
955
956
957
958
959
960
961
962
963
964
965
966
967
968
969
970
971
972
973
974
975
976
977
978
979
980
981
982
983
984
985
986
987
988
989
990
991
992
993
994
995
996
997
998
999
1000

The use of a realistic dynamical biomechanical model of the face has allowed simulating a number of facial movements comparable to those occurring during the production of speech or of facial mimics in non-verbal communication.

One of the main specificities in our model is the representation of the muscles. First, their anatomical description, which relies on subject specific medical images and anatomical data, is independent from the finite element mesh. It enables to easily modify the structure of the mesh, its number or type of elements, without losing the anatomical information. The second aspect that makes our model original is the modelling of elastic muscle properties and more specifically the stress stiffening effect associated with muscle activation. The elastic characteristics are inherent to the muscle body definition, and are determined by varying the constitutive law of the muscle's tissues with the level of activation of the muscle. Results on the protrusion movement have shown that this approach enhances the generation of accurate facial movements and shapes (Nazari et al., 2008).

Studies in the literature have shown that articulatory dynamics has a major impact on the temporal patterning of speech movements. Time characteristics are important in speech perception. We have shown that lip movement patterns are indeed different in quasi-static and dynamic simulation frameworks. Interesting results, close to experimental observations, have been obtained for the dynamic framework, and not

1
2
3 for the quasi-static one, such as the generation of curved paths and bell-shaped
4 velocity profiles classically observed in unperturbed skilled human movements
5
6 (Morasso 1981). The clear differences observed between the trajectories simulated
7
8 with dynamic and static analysis demonstrate that the usage of dynamic analysis is a
9
10 requirement for speech production studies. The role of dynamics has also been
11
12 studied in the literature for non-speech movements. Ambadar et al. (2005) observed
13
14 for example that recognition of subtle facial expressions by watching the evolution of
15
16 facial gestures in time is much easier than by looking at static shots. Hence, in
17
18 modelling studies, if temporal patterning of movements integrates dynamic
19
20 constraints like inertia and viscosity, synthetic facial expressions will be deciphered
21
22 faster and easier.
23
24
25
26
27
28

29 Simulations have also highlighted the indirect role of stiffening the face,
30 mostly in the cheeks area, on the way muscles impact the lip shapes. It was shown
31
32 that the stiffening of the cheeks due to the activation of the buccinator induces a
33
34 limitation of the amplitude of the upper lip protrusion associated with OOP activation.
35
36 The role of muscles, which are not directly involved in lip shaping, was thus
37
38 demonstrated. These results, similar to those of Buchaillard et al. (2009) about the
39
40 role of mouth floor muscles in tongue elevation, are encouraging for our modelling
41
42 approach toward a better understanding of facial mimic mechanisms.
43
44
45
46
47

48 Future improvements of the model will among others concern the mechanical
49
50 properties, to account for the non-homogeneity of the tissue layers, and include some
51
52 mesh refinement. Also, new muscle elements will be developed to integrate the
53
54 displacements and strain dynamically in their constitutive law. This will be used while
55
56 implementing a motor control mechanism that integrates voluntary commands and
57
58 low-level feedback. This mechanism will handle the activation commands sent to
59
60

1
2
3 every muscle to reach specific targets, defined as positions or shapes of the face in
4 relation with specific spectral patterns of the acoustic signal. Other works will
5 concern the coupling of the face with a model of the jaw. Finally, experimental data
6 will be more extensively used to better evaluate, qualitatively and/or quantitatively,
7 the simulated orofacial movements.
8
9
10
11
12
13
14

15 16 **Appendix**

17
18 The sparse direct solver based on Newton-Raphson method has been used.
19
20 Convergence is assumed when
21

$$22 \quad \|\Delta V\| < \varepsilon_V V_{ref}$$

23
24 where V is the variable, which is in our case either force or displacement, ε_V is the
25 tolerance and $\|\Delta V\|$ the Euclidian norm of the variable difference at each time step
26 (ANSYS Inc., Theory Reference). The assumed values are given in Table 3.
27
28
29
30
31
32
33
34

35 ----Table 3 around here-----
36
37
38
39

40 In the Newton-Raphson method, line search with adaptive descent is used. The
41 computation time on a Windows XP (32bit) platform running on a machine with a
42 Duo CPU E6850 @ 3 GHz for static analysis is around 3000 seconds per simulation
43 (3183 CPU times) and for dynamic analysis is around 20,000 seconds (10,000 CPU
44 times) for simulation of one second real time gesture.
45
46
47
48
49
50
51
52

53 **Acknowledgement**

54
55 We are pleased to express our gratitude to Dr. Pierre Badin, Dr. Christophe
56 Savariaux and Dr. Jean Luc-Schwarz for providing us with experimental movement
57 data from different subjects.
58
59
60

FIGURES CAPTIONS

Figure 1: Main mesh of the face soft tissue.

Figure 2: Surfaces of contact elements between lips (a) and lips and teeth (b).

Figure 3: Macrofibers defining the muscles of the face shown in CT data (a), in the main mesh (b), and with their abbreviated names (c).

Figure 4: Coupling elements between the piece-wise fibres of cable elements and the main mesh (only the left half of face is shown).

Figure 5: Body of the muscles: elements of the main mesh in a neighbourhood of the muscles fibres (only the left half of face is shown).

Figure 6: A schematic representation of stress stiffening effect. A point P inside a muscle at equilibrium under constant muscle activation (force F_1) (top panel) is virtually displaced by δ under the action of a transversal force F (bottom panel). Once the new equilibrium is reached with a new force level F_1 , transversal stiffness $dF/d\delta$ is proportional to that force.

Figure 7: Modelling of the stress stiffening effect: variation of the hyperelastic constitutive law of the tissue with the activation of the muscle.

Figure 8: Face shaping after activation of the zygomaticus muscle

Figure 9: Face shaping from coordinate activation of the zygomaticus, levator labii superioris alaeque nasi and levator angulai oris muscles

Figure 10: Face shaping resulting from the orbicularis oris peripheralis activation

Figure 11: Face shaping resulting from the risorius activation

Figure 12: Face shaping resulting from the buccinator activation

1
2
3 Figure 13: Face shaping resulting from the orbicularis oris peripheralis and buccinator
4 co-activation
5
6
7

8 Figure 14: Comparison between the trajectories of a point on the lower lip in the mid-
9 sagittal plane in static and dynamic analysis resulting from an orbicularis oris
10 peripheralis and mentalis co-activation (with $E_{\text{cable}}=0.3$ and $T=-500$ with spherical
11 neighbourhood radius for OOP 3mm and for MENT 2 mm).
12
13

14
15 Figure 15: Upper panel: Velocity profile of a point on the lower lip in the mid-sagittal
16 plane resulting from the co-activation of orbicularis oris peripheralis and mentalis in
17 dynamic analysis. Lower panel: Time patterns of the corresponding activations. (with
18 $E_{\text{cable}}=0.3$ and $T=-500$ with spherical neighbourhood radius for OOP 3mm and for
19 MENT 2 mm)
20

21 Figure 16: Experimental data. Top panel: trajectory of a point on the lower lip in the
22 mid-sagittal plane in /iRy/ sequence; diamond mark is for the starting point and
23 square mark for the ending point. Bottom panel: corresponding acoustic signal with
24 phonetic labelling
25

26 Figure 17: Experimental data. Tangential velocity profile corresponding to trajectory
27 and the acoustic signal displayed in Figure 16.
28
29
30
31
32
33
34
35
36
37
38
39
40
41
42
43
44
45
46
47
48
49
50
51
52
53
54
55
56
57
58
59
60

TABLES

Table 1. Constants of the simplified 5-parameter Mooney-Rivlin model for passive tissues

c_{10} (MPa)	c_{20} (MPa)	d (1/MPa)
2.5e-3	1.175e-3	0.8

Table 2. Orofacial Muscles for half of the face

Muscle Name	Abbreviation	Number of Fibres	Total Number of Cable Elements
Levator Labii Superioris Alaeque Nasi	LLSAN	2	12
Levator Anguli Oris	LAO	1	9
Zygomaticus (major and minor)	ZYG	2	15
Risorius	RIS	1	6
Buccinator	BUC	2	12
Depressor Anguli Oris	DAO	2	12
Depressor Labii Inferioris	DLI	2	11
Mentalis	MENT	2	11
Orbicularis Oris Peripheralis (Inferioris and Superioris)	OOP	2	14
Orbicularis Oris Marginalis (Inferioris and Superioris)	OOM	2	14

Table 3. Tolerance values

	ε	V_{ref}
Force (N)	0.035	0.01
Displacement (mm)	0.01	0.00

REFERENCES

- Abry C, Lallouache MT and Cathiard MA. 1996. How can coarticulation models account for speech sensitivity to audio-visual desynchronization? In *Speechreading by Humans and Machines*, NATO ASI Series F: Computer and System Sciences, Stork D & Hennecke M eds. 150:pp. 247-255. Springer-Verlag, Berlin, Heidelberg, Tokyo.
- Ambadar Z, Schooler J and Cohn JF. 2005. Deciphering the enigmatic face: the importance of facial dynamics to interpreting subtle facial expressions. *Psychological Science*. 16(5): 403-41.
- Ansys, Inc. 2007. *Theory Reference Manual*. Release 11.
- Blanton PL, Biggs NL and Perkins RC. 1970. Electromyographic analysis of the buccinator muscle. *J. Dent. Res.* 49:389-394.
- Badin P, Elisei F, Bailly G and Tarabalka Y. 2008. An audiovisual talking head for augmented speech generation: models and animations based on a real speaker's articulatory data. *Proceedings of the 5th Conference on Articulated Motion and Deformable Objects (AMDO 2008)*. Springer Verlag LNCS 5098:132-143.
- Blemker S, Pinsky PM and Delp SL. 2005. A 3D model of muscle reveals the causes of nonuniform strains in the biceps brachii. *J. of Biomechanics*. 38:657-665.
- Buchaillard S, Perrier P and Payan Y. 2006. A 3D biomechanical vocal tract model to study speech production control: How to take into account the gravity? *Proc. of the 7th International Seminar on Speech Production*, pp. 403-410.
- Buchaillard S, Perrier P and Payan Y. 2009. A biomechanical model of cardinal vowel production: Muscle activations and the impact of gravity on tongue positioning. *J. Acoustical Society of America*, 126(4):2033-2051.
- Chabanas M, Luboz V and Payan Y. 2003. Patient specific finite element model of the face soft tissues for computer-assisted maxillofacial surgery. *Medical Image Analysis*. 7:131-151.
- Feldman AG. 1986. Once more on the Equilibrium-Point hypothesis (λ model) for motor control. *J. of Motor Behavior*. 18(1):17-54.
- Fung YC. 1993. *Biomechanics: Mechanical properties of living tissues*. Springer-Verlag, New York Inc.
- Gerard JM, Ohayon J, Luboz V, Perrier P and Payan Y. 2005. Non-linear elastic properties of the lingual and facial tissues assessed by indentation technique, Application to the biomechanics of speech production. *Medical Engineering & Physics*. 27:884-892.
- Gladilin E, Ivanov A and Roginsky V. 2004. A framework for biomechanical simulation of cranio-maxillofacial surgery interventions. *Proc of International Symposium on Medical Simulation, ISMS 2004*, S. Cotin and D. Metaxas, eds., pp. 287-294.
- Gomi H, Nozoe J, Dang J and Honda K. 2006. A physiologically based model of perioral dynamics for various lip deformations in speech articulation. *Speech Production: Models, Phonetic Processes and Techniques*, J. Harrington and M. Tabain, eds., Psychology Press, pp 119-134.
- Groleau J, Chabanas M, Marécaux Ch, Payrard N, Segaud B, Rochette M, Perrier P and Payan Y. 2007. A biomechanical model of the face including muscles for the prediction of deformations during speech production. *Proceedings of the 5th International Workshop on Models and Analysis of Vocal Emissions for Biomedical Applications, MAVIBA'2007*, Firenze, Italie.

- 1
2
3
4
5
6
7
8
9
10
11
12
13
14
15
16
17
18
19
20
21
22
23
24
25
26
27
28
29
30
31
32
33
34
35
36
37
38
39
40
41
42
43
44
45
46
47
48
49
50
51
52
53
54
55
56
57
58
59
60
- Hardcastle WJ. 1976. *Physiology of Speech Production*. Academic Press, London.
- Hill AV. 1938. The heat of shortening and the dynamic constants of muscle. *Proc Royal Society, Biological Sciences*. 126:136-195.
- Humphrey JD and Yin FCP. 1989. Constitutive relations and finite deformations of passive cardiac tissue II: Stress analysis in the left ventricle. *Circulation Research*. 65:805-817.
- Lee Y, Terzopoulos D and Waters K. 1995. Realistic modeling for facial animation. SIGGRAPH'95, S.G. Mair and R. Cook, eds. New York, ACM Press, 55–62.
- Loocke MV, Lyons CG and Symms CK. 2006. A validated model of passive muscle in compression. *J. of Biomechanics*. 39:2999-3009.
- Lucero JC and Munhall KG. 1999. A model of facial biomechanics for speech production. *J. Acoust. Soc. Am*. 106:2834–2842.
- Lucero JC, Maciel STR, Johns DA and Munhall KG. 2005. Empirical modeling of human face kinematics during speech using motion clustering. *J. Acoust. Soc. Am*. 118(1): 405-409.
- McGurk H and MacDonald J. 1976. Hearing Lips and Seeing Voices. *Nature*, 264:746-48.
- McMahon TA. 1984. *Muscles, Reflexes, and Locomotion*. Princeton University Press.
- Morasso P. 1981. Spatial control of arm movements. *Exp. Brain Res*. 42:223-227.
- Munhall KG and Vatikiotis-Bateson E. 1998. The moving face during speech communication. *Hearing by Eye, Part 2: The Psychology of Speechreading and Audiovisual Speech*, edited by R. Campbell, B. Dodd, and D. Burnham. Taylor and Francis, Psychology Press, London.
- Nazari MA, Payan Y, Perrier P, Chabanas M and Lobos C. 2008. A continuous biomechanical model of the face: a study of muscle coordinations for speech lip gestures. *Proceedings of the 8th International Seminar on Speech Production, ISSP'08*, pp. 321-324.
- Ng-Thow-Hing V and Fiume E. 2002. Application-specific muscle representations. *Proc. of Gr. Inter*, W. Sturzlinger and M. McCool, editors, pp. 107–115.
- O'Shaughnessy D. 1981. A study of French vowel and consonant durations. *J. of Phonetics*. 9:385-406.
- Payan Y and Perrier P. 1997. Synthesis of V-V sequences with a 2D biomechanical tongue model controlled by the Equilibrium Point Hypothesis. *Speech Communication*. 22:185-205.
- Perrier P, Payan Y, Zandipour M and Perkell J. 2003. Influences of tongue biomechanics on speech movements during the production of velar stop consonants: A modeling study. *J. Acoustical Soc. of America*. 114(3):77–83.
- Shaiman S, Adams SG and Kimelman MDZ. 1997. Velocity profiles of lip protrusion across changes in speaking rate. *Journal of Speech, Language, and Hearing Research*. 40: 144-158.
- Sifakis E, Neverov I and Fedkiw R. 2005. Automatic Determination of Facial Muscle Activations from Sparse Motion Capture Marker Data. *ACM Transactions on Graphics (SIGGRAPH Proceedings)*.24:417-425.
- Sifakis E, Selle A, Robinson-Mosher A and Fedkiw R. 2006. Simulating Speech with a Physics-Based Facial Muscle Model. *Eurographics/ ACM SIGGRAPH*, M.P. Cani, and J.O. Brien, editors, Symposium on Computer Animation.
- Standring S. (editor in chief). 2005. *Gray's Anatomy: The Anatomical Basis of Clinical Practice*. 39th Edition, Elsevier Ltd..

- 1
2
3 Teran J, Sifakis E, Blemker S, Ng Thow Hing V, Lau C and Fedkiw R. 2005.
4 Creating and Simulating Skeletal Muscle from the Visible Human Data Set.
5 IEEE TVCG. 11:317-328.
6
7 Tracqui P and Ohayon J. 2004. Transmission of mechanical stresses within the
8 cytoskeleton of adherent cells: a theoretical analysis based on a multi-
9 component model. *Acta Biotheoretica*. 52:323-341.
10
11 Weiss JA, Maker BN and Govindjee S. 1996. Finite element implementation of
12 incompressible, transversely isotropic hyperelasticity. *Comput. Methods Appl.*
13 *Mech. Engrg.* 135:107-128.
14
15 Wilhelms-Tricario R. 1995. Physiological modeling of speech production: methods
16 for modeling soft-tissue articulators. *J. Acoustical Society of America*.
17 97:3085–3098.
18
19 Yucesoy CA, Koopman BHFJM, Huijing PA and Grootenboer HJ. 2002. Three-
20 dimensional finite element modeling of skeletal muscle using a two-domain
21 approach: linked fibre-matrix mesh model. *J. of Biomechanics*. 35:1253-1262.
22
23 Zajac F. 1989. Muscle and tendon: Properties, models, scaling, and application to
24 biomechanics and motor control. *Critical Reviews in Biomed. Eng.* 17:359–
25 411.
26
27
28
29
30
31
32
33
34
35
36
37
38
39
40
41
42
43
44
45
46
47
48
49
50
51
52
53
54
55
56
57
58
59
60

1
2
3
4
5
6
7
8
9
10
11
12
13
14
15
16
17
18
19
20
21
22
23
24
25
26
27
28
29
30
31
32
33
34
35
36
37
38
39
40
41
42
43
44
45
46
47
48
49
50
51
52
53
54
55
56
57
58
59
60

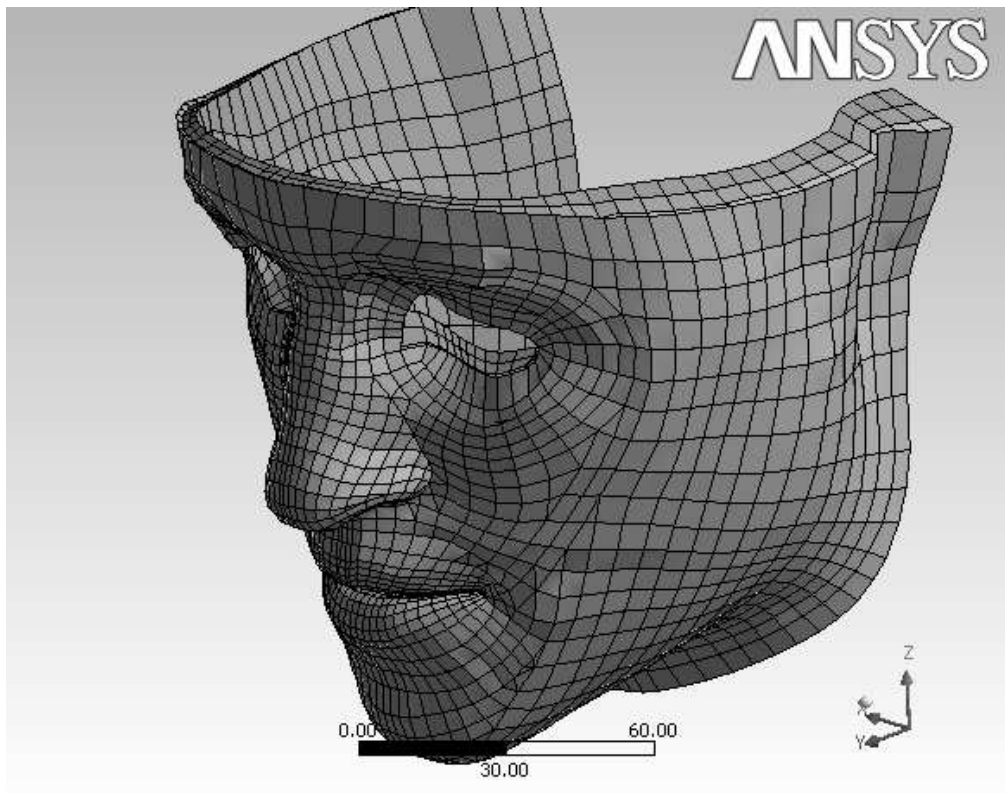


Figure 1: Main mesh of the face soft tissue.
204x164mm (72 x 72 DPI)

Preview Only

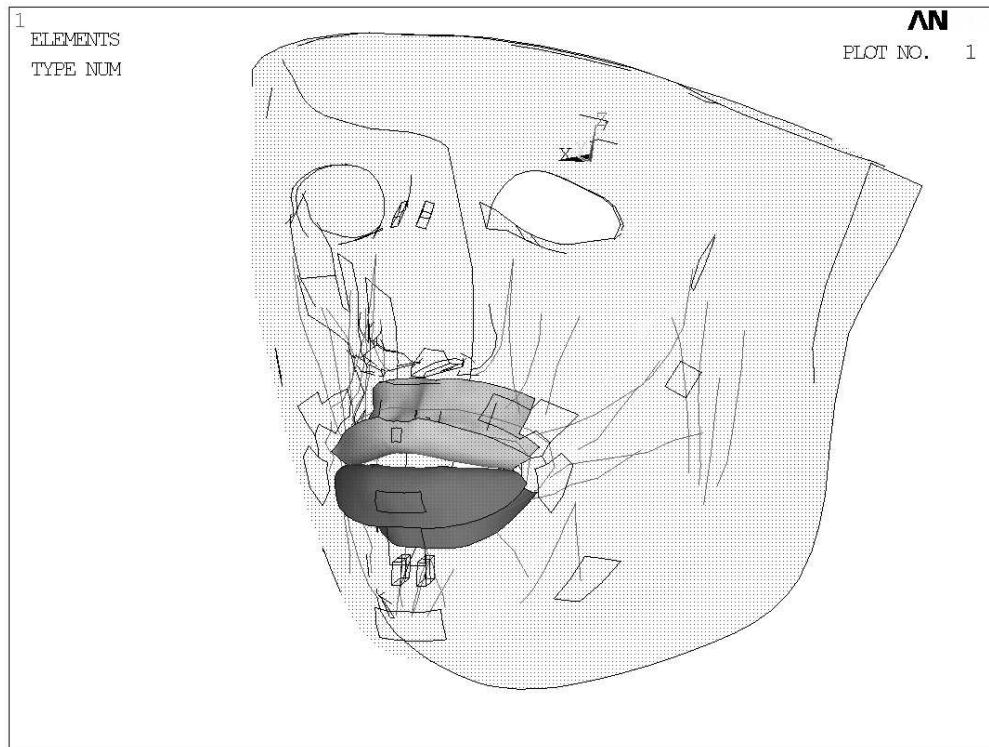
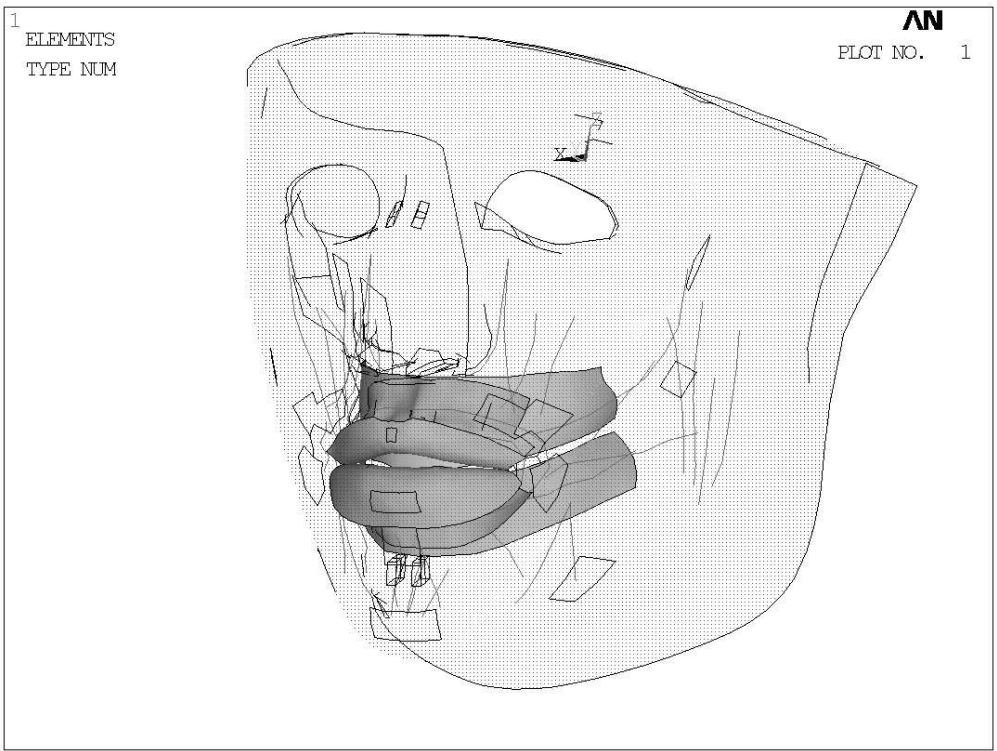


Figure 2: Surfaces of contact elements between lips (a)
379x285mm (72 x 72 DPI)

1
2
3
4
5
6
7
8
9
10
11
12
13
14
15
16
17
18
19
20
21
22
23
24
25
26
27
28
29
30
31
32
33
34
35
36
37
38
39
40
41
42
43
44
45
46
47
48
49
50
51
52
53
54
55
56
57
58
59
60



and lips and teeth (b).
379x285mm (72 x 72 DPI)

new Only

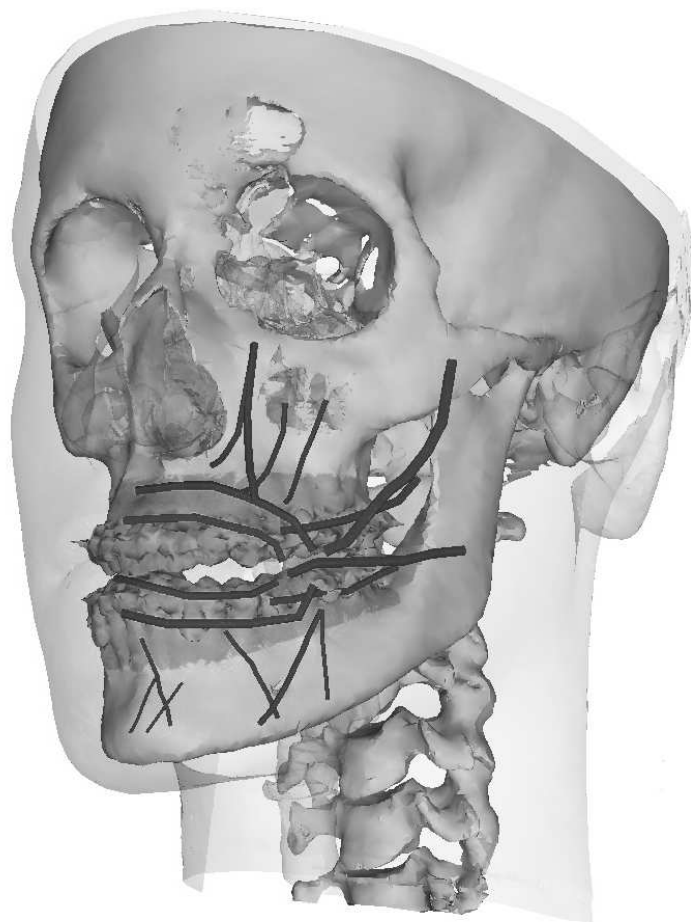
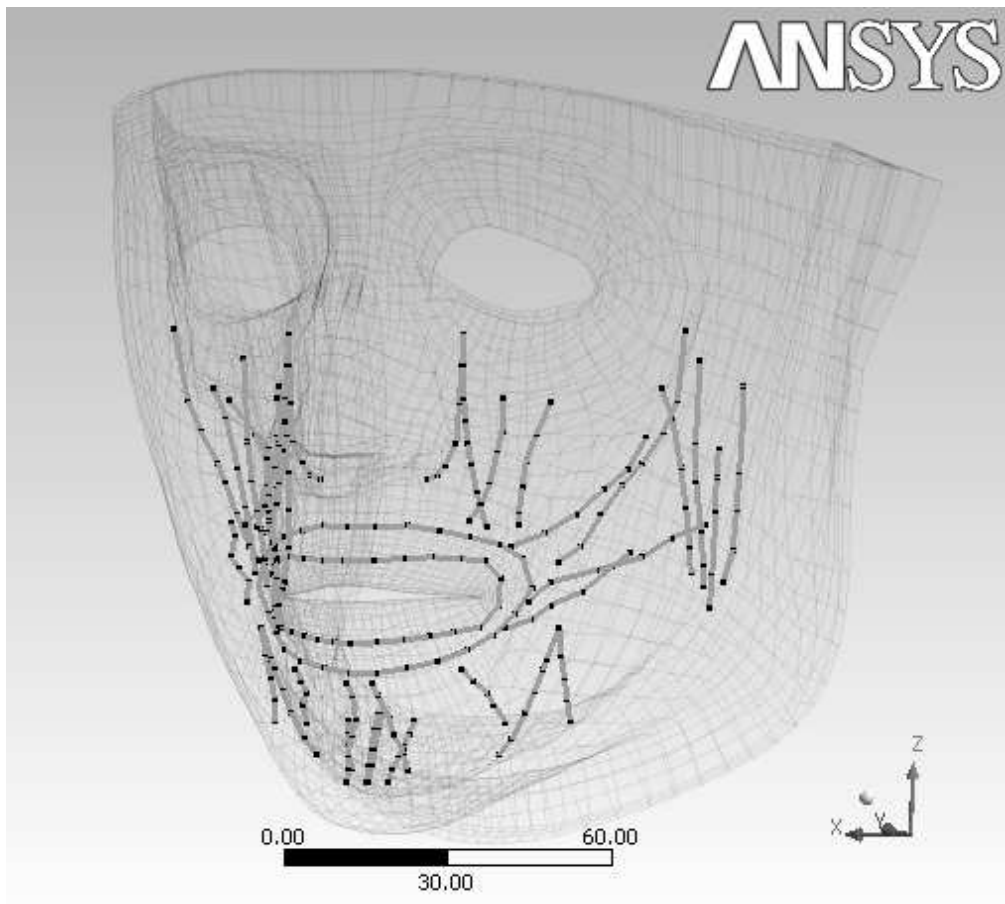


Figure 3: Macrofibers defining the muscles of the face shown in CT data (a),
340x351mm (72 x 72 DPI)

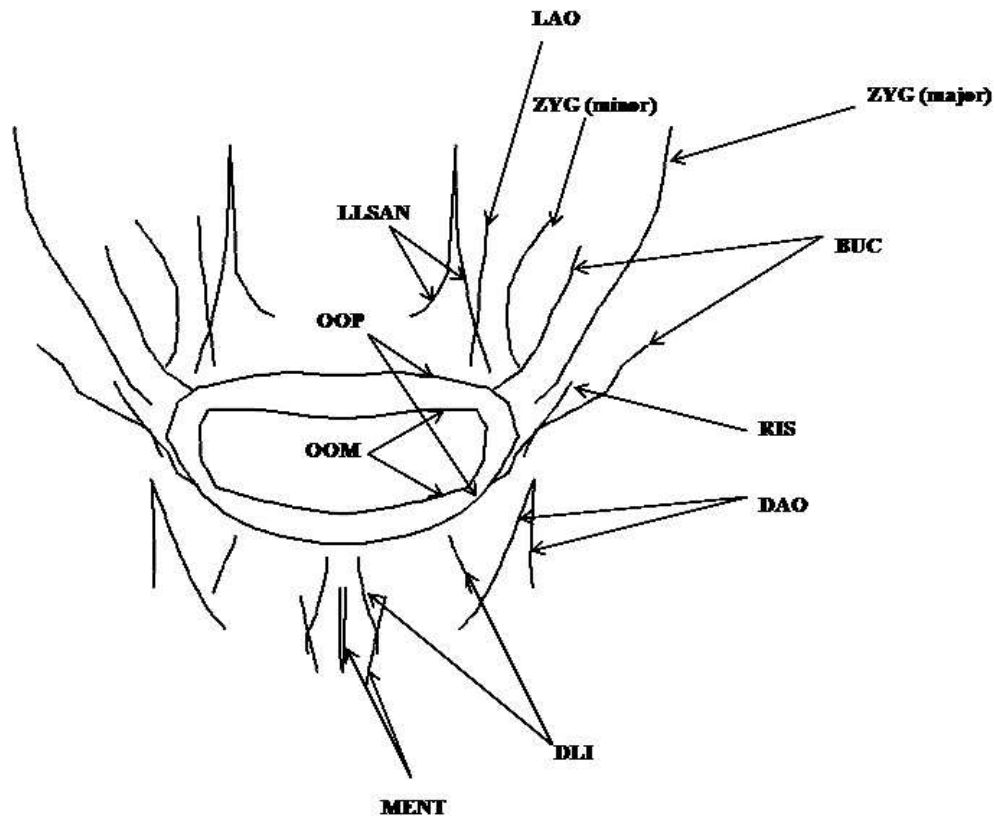


1
2
3
4
5
6
7
8
9
10
11
12
13
14
15
16
17
18
19
20
21
22
23
24
25
26
27
28
29
30
31
32
33
34
35
36
37
38
39
40
41
42
43
44
45
46
47
48
49
50
51
52
53
54
55
56
57
58
59
60



in the main mesh (b),
178x160mm (72 x 72 DPI)

Only



and with their abbreviated names (c).
245x202mm (72 x 72 DPI)

1
2
3
4
5
6
7
8
9
10
11
12
13
14
15
16
17
18
19
20
21
22
23
24
25
26
27
28
29
30
31
32
33
34
35
36
37
38
39
40
41
42
43
44
45
46
47
48
49
50
51
52
53
54
55
56
57
58
59
60

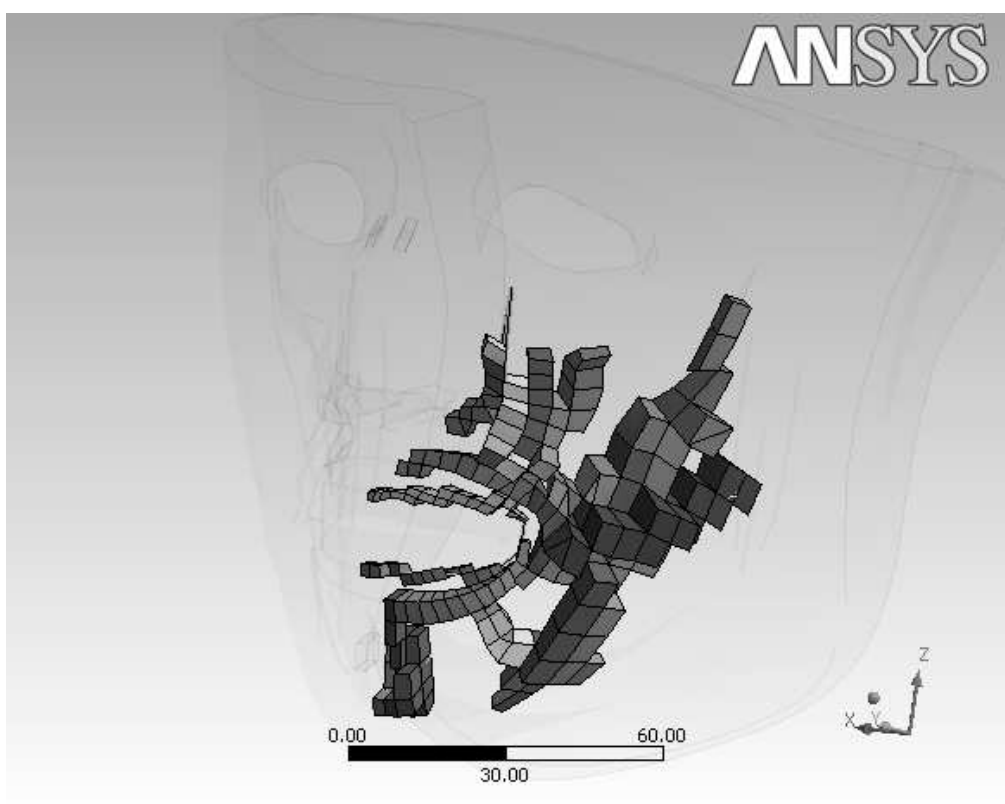


Figure 4: Coupling elements between the piece-wise fibres of cable elements and the main mesh (only the left half of face is shown).
204x164mm (72 x 72 DPI)

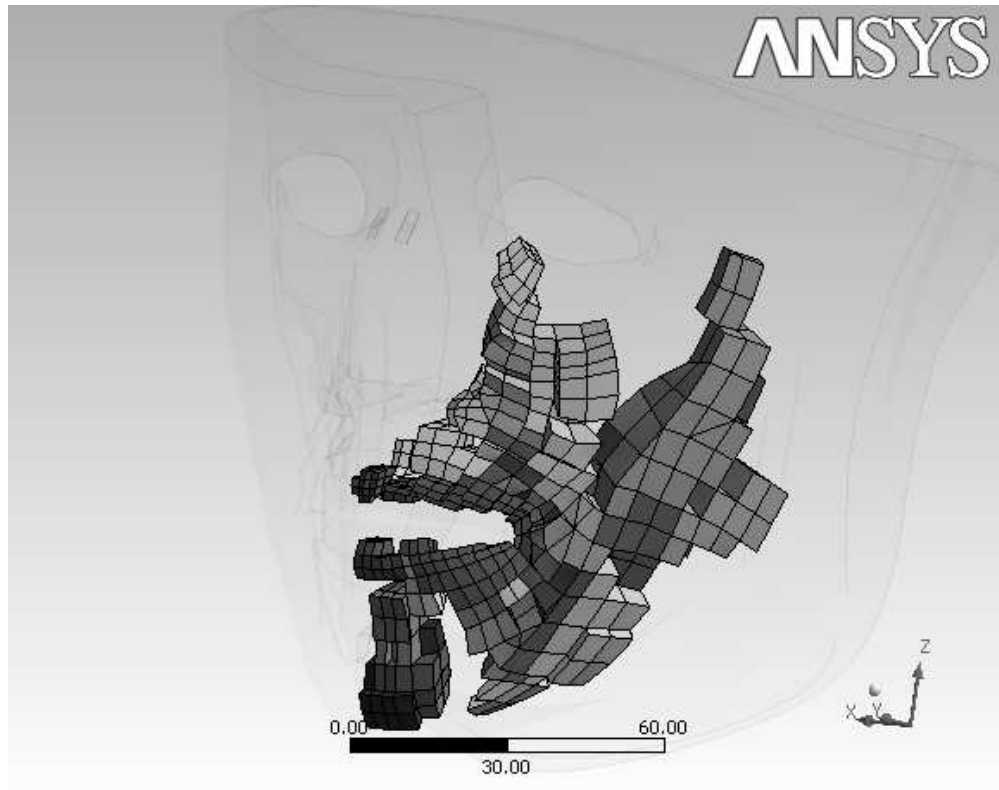


Figure 5: Body of the muscles: elements of the main mesh in a neighbourhood of the muscles fibres (only the left half of face is shown).
204x164mm (72 x 72 DPI)

1
2
3
4
5
6
7
8
9
10
11
12
13
14
15
16
17
18
19
20
21
22
23
24
25
26
27
28
29
30
31
32
33
34
35
36
37
38
39
40
41
42
43
44
45
46
47
48
49
50
51
52
53
54
55
56
57
58
59
60

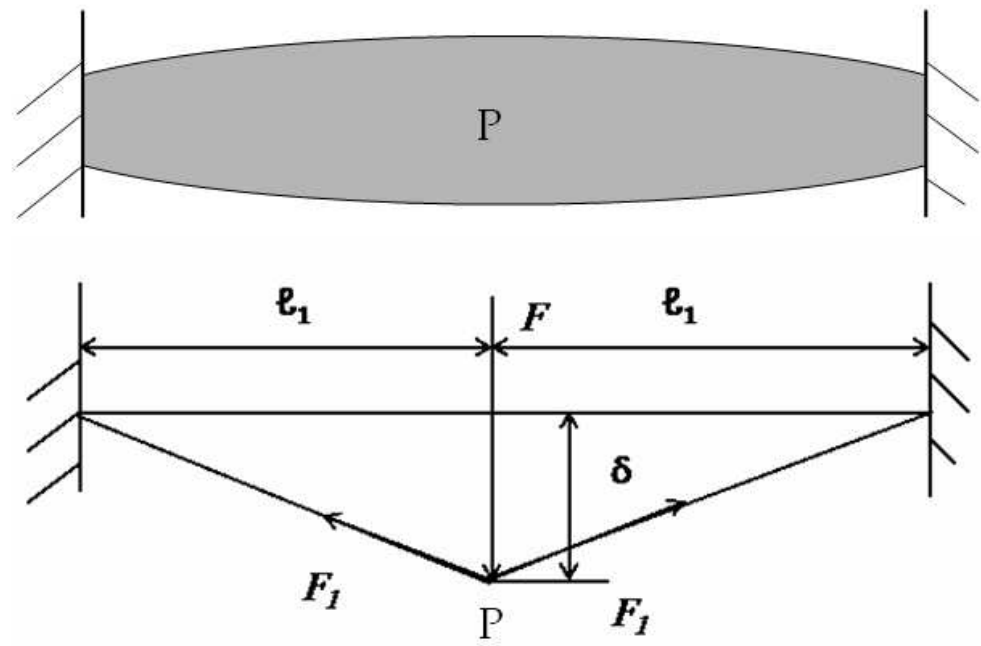
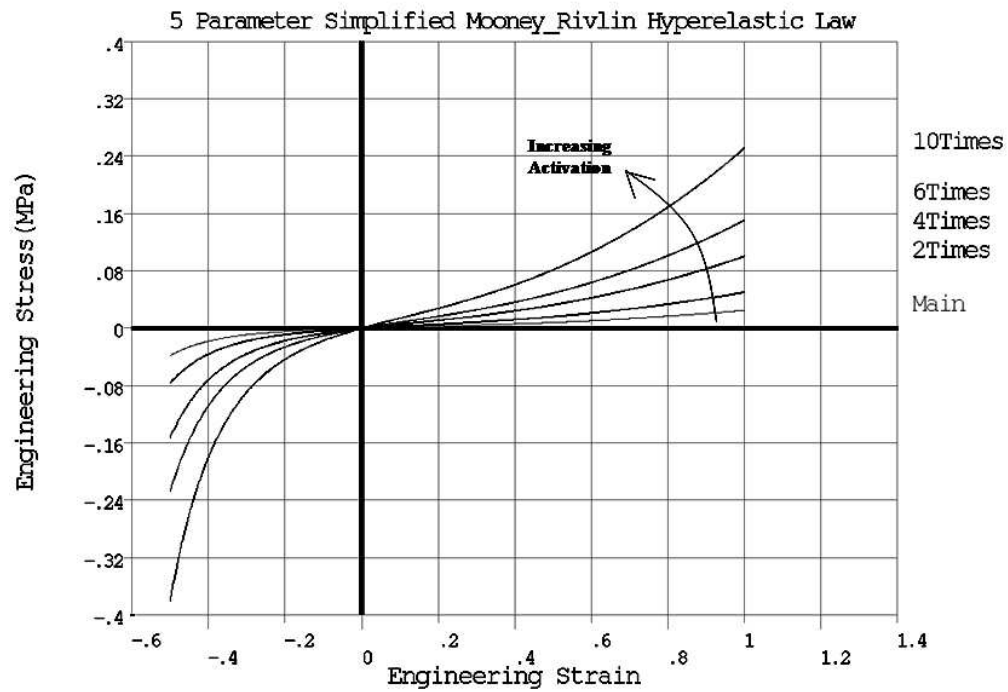


Figure 6: A schematic representation of stress stiffening effect. A point P inside a muscle at equilibrium under constant muscle activation (force F_1) (top panel) is virtually displaced by δ under the action of a transversal force F (bottom panel). Once the new equilibrium is reached with a new force level F_1 , transversal stiffness $dF/d\delta$ is proportional to that force.

219x144mm (72 x 72 DPI)



32 Figure 7: Modelling of the stress stiffening effect: variation of the hyperelastic constitutive law of
33 the tissue with the activation of the muscle.
34 291x206mm (72 x 72 DPI)

1
2
3
4
5
6
7
8
9
10
11
12
13
14
15
16
17
18
19
20
21
22
23
24
25
26
27
28
29
30
31
32
33
34
35
36
37
38
39
40
41
42
43
44
45
46
47
48
49
50
51
52
53
54
55
56
57
58
59
60

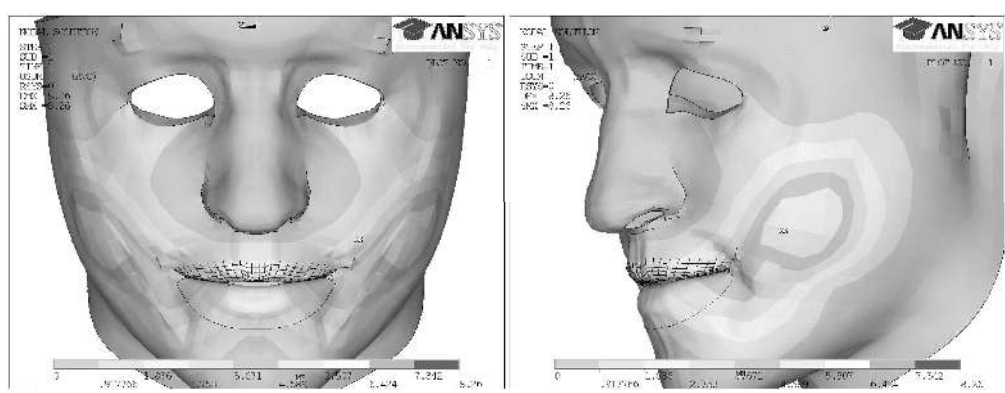


Figure 8: Face shaping after activation of the zygomaticus muscle
759x285mm (72 x 72 DPI)

Peer Review Only

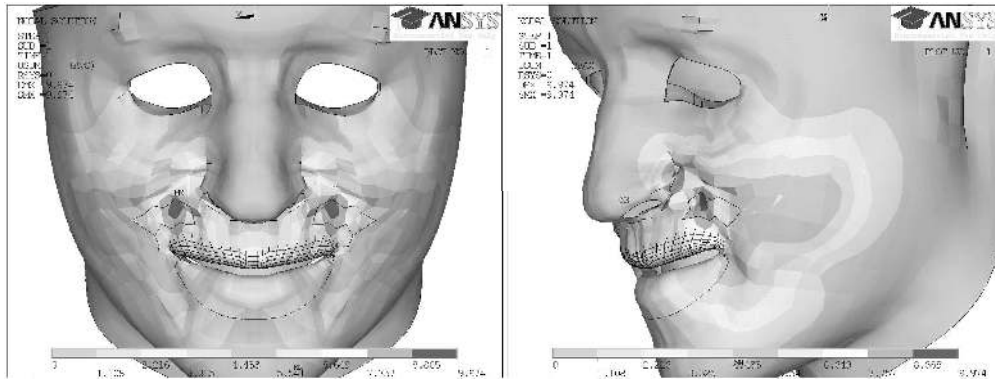


Figure 9: Face shaping from coordinate activation of the zygomaticus, levator labii superioris alaeque nasi and levator angulai oris muscles
759x285mm (72 x 72 DPI)

1
2
3
4
5
6
7
8
9
10
11
12
13
14
15
16
17
18
19
20
21
22
23
24
25
26
27
28
29
30
31
32
33
34
35
36
37
38
39
40
41
42
43
44
45
46
47
48
49
50
51
52
53
54
55
56
57
58
59
60

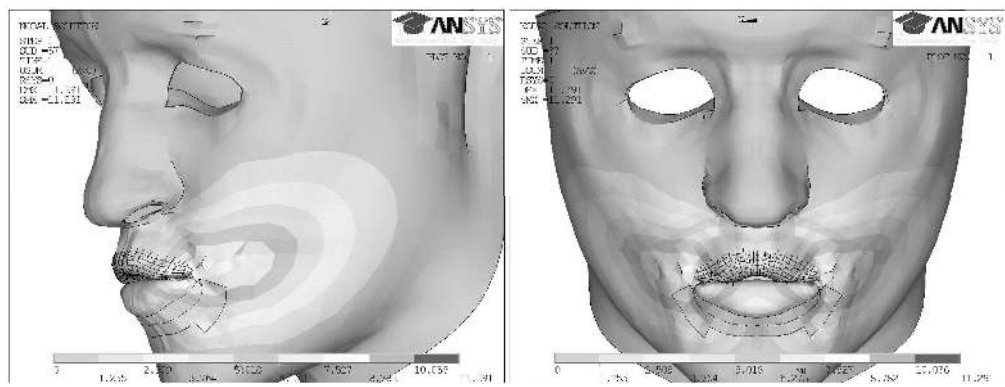


Figure 10: Face shaping resulting from the orbicularis oris peripheralis activation
759x285mm (72 x 72 DPI)

Peer Review Only

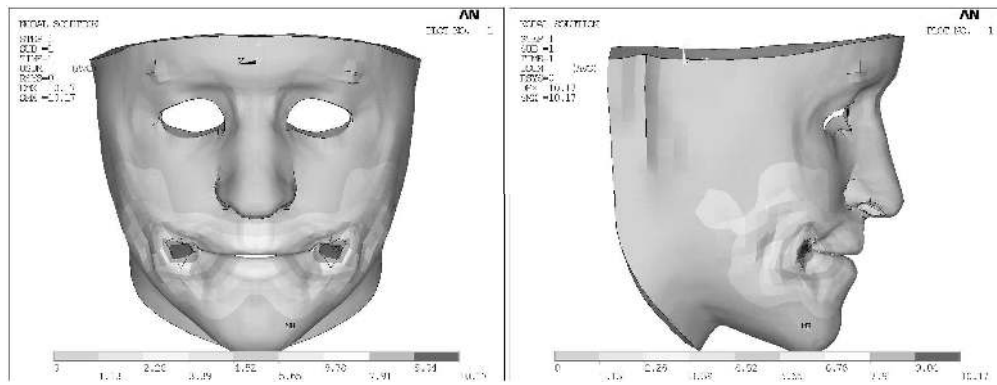


Figure 11: Face shaping resulting from the risorius activation
759x285mm (72 x 72 DPI)

1
2
3
4
5
6
7
8
9
10
11
12
13
14
15
16
17
18
19
20
21
22
23
24
25
26
27
28
29
30
31
32
33
34
35
36
37
38
39
40
41
42
43
44
45
46
47
48
49
50
51
52
53
54
55
56
57
58
59
60

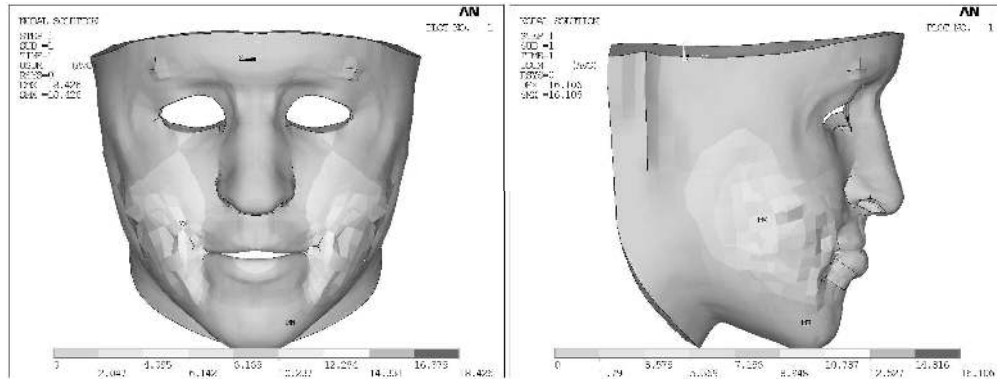


Figure 12: Face shaping resulting from the buccinator activation
759x285mm (72 x 72 DPI)

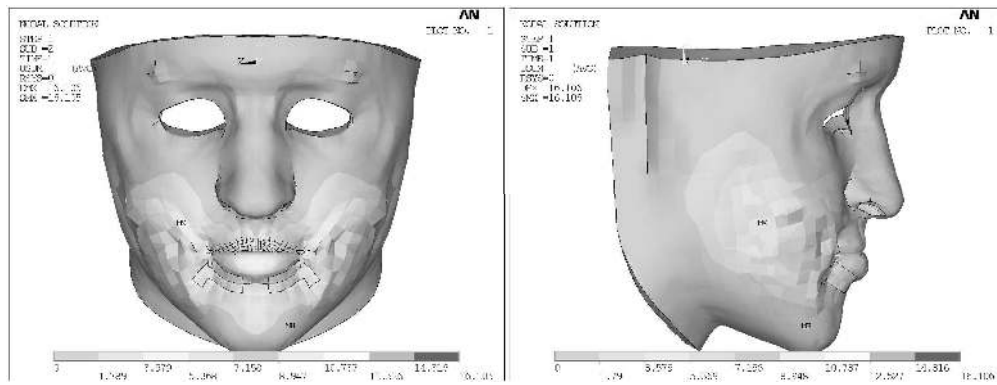


Figure 13: Face shaping resulting from the orbicularis oris peripheralis and buccinator co-activation
759x285mm (72 x 72 DPI)

1
2
3
4
5
6
7
8
9
10
11
12
13
14
15
16
17
18
19
20
21
22
23
24
25
26
27
28
29
30
31
32
33
34
35
36
37
38
39
40
41
42
43
44
45
46
47
48
49
50
51
52
53
54
55
56
57
58
59
60

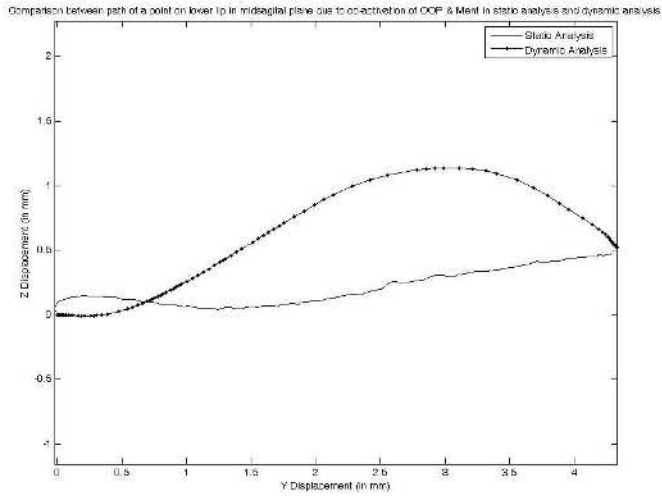


Figure 14: Comparison between the trajectories of a point on the lower lip in the mid-sagittal plane in static and dynamic analysis resulting from an orbicularis oris peripheralis and mentalis co-activation (with $E_{cable}=0.3$ and $T=-500$ with spherical neighbourhood radius for OOP 3mm and for MENT 2 mm).
338x184mm (96 x 96 DPI)

Review Only

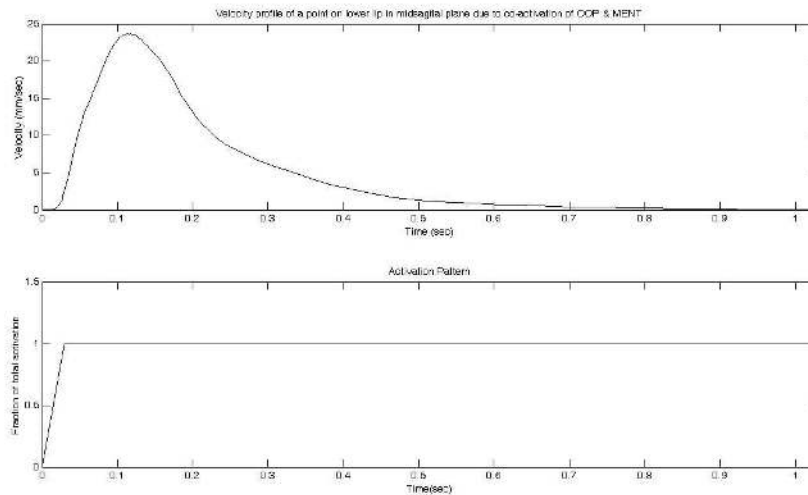


Figure 15: Upper panel: Velocity profile of a point on the lower lip in the mid-sagittal plane resulting from the co-activation of orbicularis oris peripheralis and mentalis in dynamic analysis. Lower panel: Time patterns of the corresponding activations. (with $E_{cable}=0.3$ and $T=-500$ with spherical neighbourhood radius for OOP 3mm and for MENT 2 mm).
338x184mm (96 x 96 DPI)

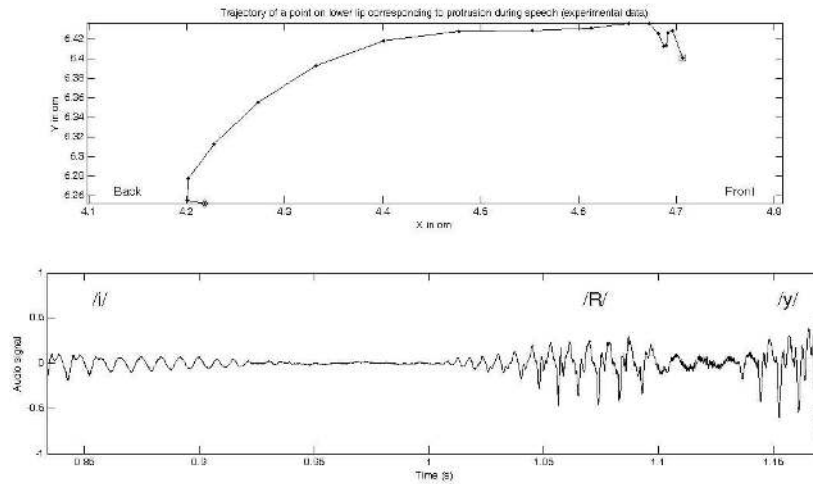


Figure 16: Experimental data. Top panel: trajectory of a point on the lower lip in the mid-sagittal plane in /iRy/ sequence; diamond mark is for the starting point and square mark for the ending point. Bottom panel: corresponding acoustic signal with phonetic labelling.
338x178mm (96 x 96 DPI)

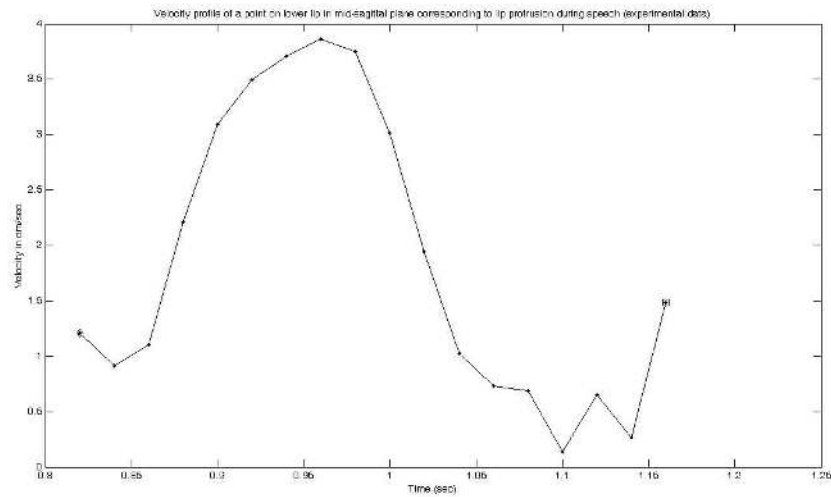


Figure 17: Experimental data. Tangential velocity profile corresponding to trajectory and the acoustic signal displayed in Figure 16.
338x184mm (96 x 96 DPI)